of the order of 10% of the 4-hr gamma rays. No such transition has been observed.

ACKNOWLEDGMENTS

The authors wish to thank Dr. R. G. Cochran for assistance in the early phase of this work and J. A. Martin and A. R. Sattler for help in taking some of the data. They also acknowledge the cooperation of F. J. Remick and others of the Pennsylvania State University Reactor staff and are grateful to Dr. H. J. van den Bold and Dr. E. A. Wolicki for the communication of their results.

PHYSICAL REVIEW VOLUME 124, NUMBER 5 DECEMBER 1, 1961

Differential Cross Sections for $(n,n'\gamma)$ Reactions in Several Nuclei*

J. W. Boring† and M. T. McEllistrem
University of Kentucky, Lexington, Kentucky

(Received June 19, 1961; revised manuscript received August 22, 1961)

Differential cross sections for the production of gamma rays by inelastic neutron scattering have been measured and compared with the predictions of the statistical model, employing a diffuse surface complex potential to represent the neutron-nucleus interaction. Transitions have been observed in Mg^{24}, Mn^{55}, Fe^{56}, and Pb^{206}. Predictions of the statistical model were in good agreement with total $(n,n'\gamma)$ cross sections measured for first-excited state transitions in Fe^{56} and Mg^{24}, and in agreement with measured transition rates from the second and third excited states of Fe^{56}. Angular distributions for Mn^{55} transitions are consistent with recent spin assignments for the second and third excited states, but the comparisons of the measured and calculated total cross sections are not as satisfactory as the comparisons in Fe^{56} and Mg^{24}.

INTRODUCTION

DIFFERENTIAL cross sections for the production of gamma rays from inelastic neutron scattering have recently been measured for several nuclei,[1–5] and these measurements have been compared to the expectations of the statistical model for nuclear reactions.[6] Within the framework of this model the differential cross sections depend only upon the form of the potential chosen to represent the neutron-nucleus interaction. The comparisons mentioned showed good agreement with the assumption of the diffuse surface potential of Beyster *et al.*[7] Comparisons of measured and calculated cross sections were also made[3,5] for the assumption of a complex square-well potential, the diffuse surface potential of Emmerich and also that of Campbell *et al.* The success of the diffuse well model in representing the measurements led Day and Walt[2] to suggest that these reactions might serve as a useful spectroscopic tool for bound states of nuclei.

The purpose of the measurements reported here was to further test the $(n,n'\gamma)$ reactions with respect to their use in nuclear spectroscopy. This was done by exciting states which produced gamma-ray transitions between states of known spin and parity. The length of time required to study a particular transition limited the number of nuclei studied to four, and the number of gamma-ray lines studied as a function of angle to six. The four nuclei chosen for study were selected to cover a large range of mass number. In selecting the nuclei to test the statistical model, interest centered on even-even nuclei. Consideration of the production cross sections, gamma-ray energy, atomic density, isotopic purity, and gamma-ray self-absorption influenced the choice of nuclei. Among transitions selected were those from the first-excited states to the ground states of Fe^{56}, Mg^{24}, and Pb^{206}, and the second to first excited state transition in Pb^{206}. For these transitions differential cross-section measurements were made at five angles between 0° and 90°. Two other transitions in Fe^{56}, one between the second and first excited states and the other between the third and first excited states were also observed at 90°.

Transitions from the second and third excited states of Mn^{55} were studied in order to provide additional information relevant to the determination of the spins of those states.

EXPERIMENTAL APPARATUS AND PROCEDURE

Neutrons of approximately 2.9 Mev were produced at a 180-kev deuteron accelerator via the $D(d,n)He^3$ re-

* This work was partially supported by the U. S. Atomic Energy Commission.

† Now at the Research Laboratories for the Engineering Sciences, University of Virginia, Charlottesville, Virginia.

[1] R. B. Day, Phys. Rev. **102**, 767 (1956).

[2] R. B. Day and M. Walt, Phys. Rev. **117**, 1330 (1960).

[3] M. Hosoe and S. Suzuki, J. Phys. Soc. Japan **14**, 699 (1959).

[4] L. Cranberg and J. Levin, Phys. Rev. **103**, 343 (1956).

[5] D. M. Patter and R. W. Jackiw, *Proceedings of the International Conference on Nuclear Structure, Kingston* (University of Toronto Press, Toronto and North Holland Publishing Company, Amsterdam, 1960), p. 244. D. M. Van Patter, Bull. Am. Phys. Soc. **6**, 47 (1961). S. M. Shaforth, R. W. Jackiw, and D. M. Van Patter, Bull. Am. Phys. Soc. **5**, 409 (1960).

[6] G. R. Satchler, Phys. Rev. **94**, 1304 (1954); **104**, 1198 (1956); **111**, 1747 (1958). S. Devons and L. J. B. Goldfab, *Handbuch der Physik*, edited by S. Flügge (Springer-Verlag, Berlin, 1957), Vol. 42.

[7] J. R. Beyster, R. G. Schrandt, M. Walt, and E. W. Salmi, Los Alamos Scientific Laboratory Report LA-2099, 1957 (unpublished).

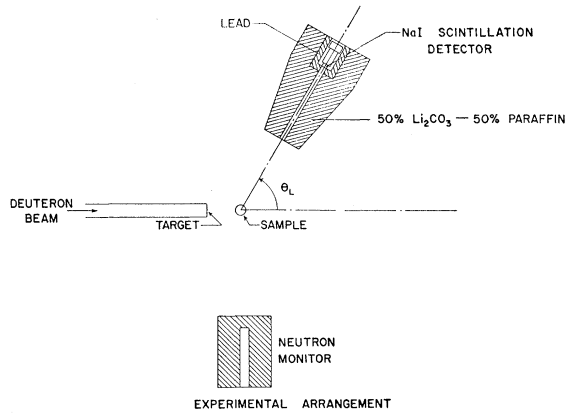

FIG. 1. Arrangement of equipment, not to any scale. 2.92-Mev neutrons from the $D(d,n)He^3$ reaction are incident upon the cylindrical scattering sample. The shielded NaI(Tl) detector rotated about the sample axis at a distance of 70 cm from the sample. The neutron monitor is a BF_3 proportional counter encased in a block of paraffin.

action. Deuterons were incident upon a thick TiD target,[8] so that the energy distribution of the neutrons from the source was approximately triangular in shape with a full width at half-maximum of 170 kev. The deuteron energy ranged from 140 to 180 kev for different samples, so that the neutron energy varied from 2.87 to 2.92 Mev. Previous measurements[4] of gamma-ray distributions in $(n,n'\gamma)$ reactions had indicated that large anisotropies might be observed at small angles. For this reason, a special effort was made to include measurements at 0° and 20°.

To make these measurements we adopted a technique used earlier by Day.[9] A pulsed neutron flux is provided by terminal pulsing the deuteron beam. The prompt gamma rays following inelastic neutron scattering are detected in coincidence with the deuteron pulses at the target. The terminal pulsing assembly follows the design described by Good,[10] except for minor modifications. The experimental arrangement is shown in Fig. 1. The pulsed neutron flux is incident upon a cylindrical sample and the radiation from the sample is detected with a shielded $1\frac{1}{2}$ in.$\times$1 in. NaI(Tl) detector; the shield design is that of Cranberg and Levin.[4] The time distribution of radiation from the neutron-producing target and sample may be displayed on a 256-channel analyzer with the aid of a time-to-pulse-height converter; the converter is a modified form of that designed by Neiler.[10] A time spectrum obtained with the detector at an angle of 0° with respect to the deuteron beam is shown in Fig. 2. The detector-to-sample distance was 70 cm, so that prompt gamma rays were separated from incident neutrons by 28 nanosec at the detector. The peak in channel 110 represents the prompt gamma rays from the neutron source and from the Fe sample; the group in channel 94 represents incident and elastically scattered neutrons.

The operating time resolution of the coincidence system was 13 nanosec; this is the full width at half-maximum of the groups in Fig. 2. Eleven nanosec of this width is the contribution of the deuteron pulse duration at the target, and the remainder is the result of the detection electronics. Under these conditions, the accelerator provided an average beam current of 6 μa with a duty cycle of 3.7%. The average neutron flux in the direction of the sample was 1.5×10^5 neutrons/sec-sr.

The procedure used was to gate the gamma-ray energy spectrum of the NaI(Tl) detector with the prompt gamma peak of Fig. 2. In this manner all of the background contained in the neutron peak and 90% of the background not correlated in time with the deuteron pulses were eliminated from the energy spectrum of the detector. This background separation enabled us to complete measurements from 0° to 90°. Samples of naturally occurring isotopic abundance were used for Fe, Mg, and Mn. The Pb sample was radio-lead[11] whose Pb^{206} concentration is quoted as 88.24%. The measured yields were corrected for the isotopic abundances of the samples. Cylindrical samples with diameters between $\frac{3}{4}$ in. and 1 in. were positioned with their axes perpendicular to the reaction plane so that the angular resolutions were: $\pm15°$ for Fe, $\pm18°$ for Mg, and $\pm27°$ for Mn and Pb. Data collection times were determined to provide statistical uncertainties of $\pm6\%$ or less; individual runs varied from 10 to 20 hr. In spite of the co-

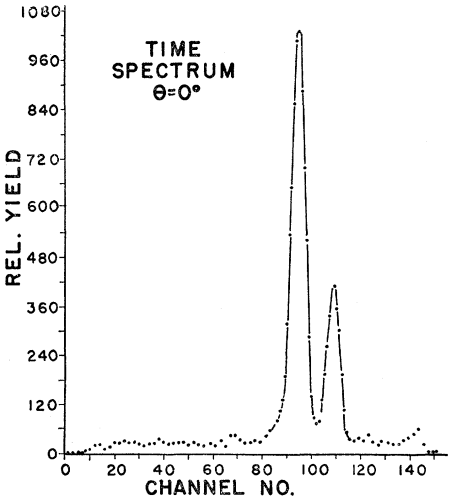

FIG. 2. Time spectrum of radiation from NaI(Tl) detector for $\theta_L=0°$. The peak in channel 110 represents prompt gamma rays from the neutron source and sample. The peak in 94 represents neutrons from the source. The full width at half-maximum of either group is 13 nanosec and they are separated by 28 nanosec.

[8] Available from Scientific Engineering Laboratories, 1510 Sixth Street, Berkeley 10, California.

[9] Joan M. Freeman, Proceedings of the International Conference on Neutron Interactions [U. S. Atomic Energy Commission Report TID-7547, 1957 (unpublished), p. 176].

[10] See *Fast Neutron Physics*, edited by J. B. Marion and J. L. Fowler (Interscience Publishers, Inc., New York, 1960), Part I, Chap. IV.

[11] Radio-lead is available from the Atomic Energy of Canada, Limited. It has the following isotopic analysis: Pb^{204}, 0.06%; Pb^{206}, 88.24%; Pb^{207}, 8.78%; Pb^{208}, 2.92%.

incidence requirement, large backgrounds were a major source of uncertainty for the relative cross-section measurements. Most of this background was prompt gamma rays from the neutron source and it was especially pronounced at small angles.

The absolute cross sections for the production of gamma rays were determined by absolute measurements of the neutron flux incident upon the sample, the gamma-ray yield, and the number of scattering nuclei within the sample. The photopeak efficiency of the $1\frac{1}{2}$-in. diameter $\times$ 1-in. thick NaI(Tl) detector was measured at 0.511 Mev and 1.277 Mev with the aid of a standard Na^{22} source placed at the normal sample position. By interpolation, a photopeak efficiency of $16.2\pm0.4\%$ was obtained at 0.662 Mev, which is in excellent agreement with the results of Bell.[12] The neutron flux was determined by simultaneously counting the neutrons and He^3 particles from the $D(d,n)He^3$ source reaction. Neutrons were counted with both a plastic scintillator and a BF_3 proportional counter encased in a block of paraffin. The He^3 particles were detected with a thin CsI(Tl) scintillator. The BF_3 counter, shown in Fig. 1, served as the flux monitor and was calibrated in terms of the He^3 counting rate. The plastic scintillator was used to measure the excitation function and angular distribution of the thick-target neutron yields. Uncertainties in the determination of the neutron flux are associated with measurements of the angular distribution of neutron yields from the $D(d,n)He^3$ reaction, solid angle of the recoil detector, and the excitation function for the $D(d,n)$ reaction from 0 to 180 kev. The combination of uncertainties in these quantities yields a neutron flux uncertainty of $\pm5.5\%$, including an estimated uncertainty of $\pm3.5\%$ attributed to the method used to correct for neutron multiple scattering. According to a calculation of Day,[1] the increase in neutron flux available for inelastic neutron scattering caused by multiple scattering is approximately equal to the attenuation in the neutron flux caused by single scattering. Day's detailed computation of multiple scattering corrections for a large number of samples yielded agreement with this simple assumption to within $\pm3.5\%$, and we have adopted it to correct for neutron absorption and multiple scattering at a gamma-ray observation angle of 90°. A final $\pm2.7\%$ uncertainty is attributed to the determination of the solid angle of the sample at the NaI(Tl) detector and additional uncertainties arising from the finite size of the sample. A total systematic uncertainty of $\pm6.7\%$ attributed to the absolute cross-section determinations was obtained as the square root of the sum of squares of the uncertainties in detector efficiency, detector solid angle, and neutron flux. This uncertainty was common to all differential cross-section measurements, and was added algebraically to the statistical and background separation uncertainties on each measurement to obtain the total uncertainty of the differential cross sections.

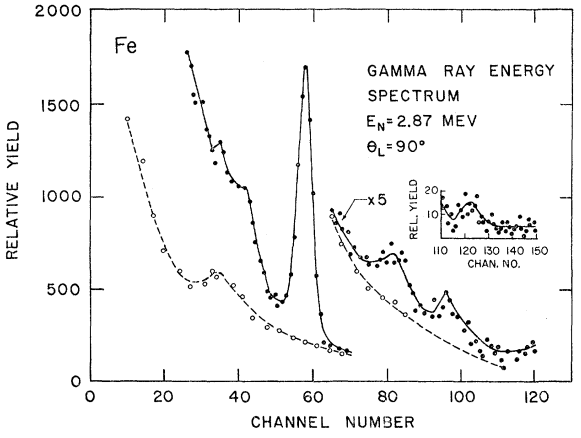

FIG. 3. Gamma-ray energy spectrum from a natural Fe sample at 90°. The photopeaks in channels 58, 82, and 122 are Fe^{56} transitions of 0.85 ± 0.015, 1.22 ± 0.03, and 1.78 ± 0.06 Mev, respectively. The photopeak in channel 96 is the first excited-to-ground state transition in Fe^{54} at 1.43 ± 0.04 Mev.

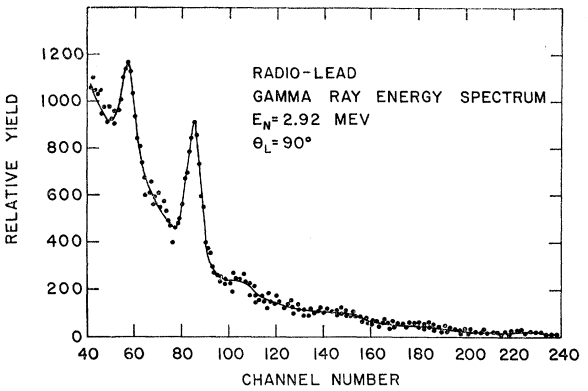

FIG. 4. 90° energy spectrum of gamma rays from the radio-lead sample. The photopeaks in channels 57 and 85 are transitions in Pb^{206} at 0.536 ± 0.007 Mev and 0.814 ± 0.01 Mev, respectively.

RESULTS

Gamma-ray spectra from $(n,n'\gamma)$ reactions in Fe, Mg, Mn, and Pb^{206} have already been published[1,3,13]; Figs. 3 and 4 are 90° energy spectra of gamma rays from the Fe and radio-lead samples, respectively. These spectra are reproduced to demonstrate the capacity of the system for these measurements. Figure 3 shows three transitions in Fe^{56} and one in Fe^{54}. The Fe^{56} transitions are at 0.85 Mev in channel 58, 1.22 Mev in channel 82, and 1.78 Mev in channel 122, shown in an inset of Fig. 3. Measurements at other angles have been made only for the strong 0.85-Mev line; small-angle backgrounds make distribution measurements of the weaker lines less feasible. Both of the prominent lines in Fig. 4 have been studied as a function of angle. The 0.536-Mev transition

[12] *Beta and Gamma-Ray Spectroscopy*, edited by K. Siegbahn (North-Nolland Publishing Company, Amsterdam, 1955).

[13] F. I. Boley, E. H. Thorndike, and A. T. Moffet, Phys. Rev. **110**, 915 (1958).

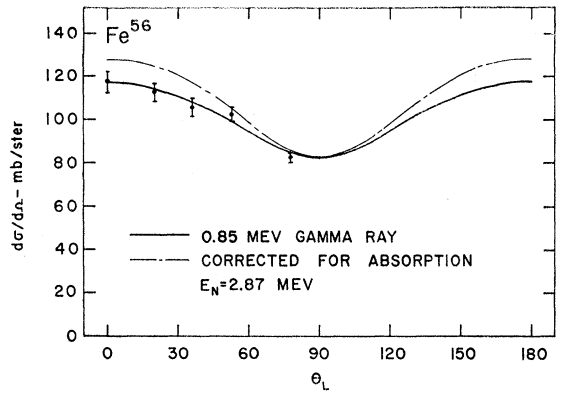

FIG. 5. Differential cross sections for the 0.85-Mev transition, showing the angular dependence of absorption corrections. The points are normalized to the corrected value of the differential cross section at 90°. The solid curve is a least-squares fit to the points. The dot-dash curve is the least-squares fit after inclusion of the angular dependence of the correction for sample absorption of neutrons and gamma rays.

in channel 57 contains a contribution from the 0.57-Mev transition in Pb^{207}. The isotopic abundance of Pb^{207} in the radio-lead sample is 8.78%[11] and the ratio of the $(n,n'\gamma)$ cross sections at 90° and at $E_n=2.56$ Mev is $\sigma(207)/\sigma(206)=1.66$.[1] We estimate, therefore, that 14% of the measured yield is a Pb^{207} contribution. Since the distribution of the Pb^{207} gamma ray has not been measured, we corrected our measurements by assuming isotropy for the Pb^{207} transition. The measured differential cross sections for the 0.85-Mev line in Fe^{56} and the 0.81-Mev line in Pb^{206} are shown in Figs. 5 and 6. The points are measured yields plotted before correction for the angular dependence of the sample absorption of neutrons and gamma rays, and the uncertainties shown are those which would vary from angle to angle, including the statistical uncertainties. The solid curves are least-squares fits to the measurements, and the dot-dash curve is the least-squares fit to the measurements after they have been corrected for the angular variation of neutron and gamma-ray absorption by the sample. The

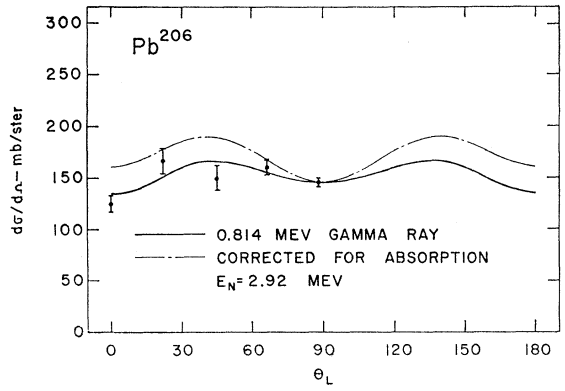

FIG. 6. Differential cross sections for the 0.814-Mev transition in Pb^{206}. The description of the curves and point plotting follows that of Fig. 5.

TABLE I. Coefficients of a least-squares fit to the differential cross sections, expanded in terms of Legendre polynomials. Coefficients are in millibarns per steradian.

Isotope	E_γ (Mev)	a_0	a_2	a_4
Fe^{56}	0.85	100.0	32.7	−5.50
Mg^{24}	1.37	53.4	−0.41	−21.5
Mn^{55}	0.861	28.3	3.96	−5.06
	1.18	24.8	5.16	−7.54
Pb^{206}	0.536	73	2.15	−26.3
	0.814	169	23.9	−32.6

absorption corrections have been calculated numerically with the aid of an IBM-650 computer. Absorption corrections at 90° have been made using the assumption of Day[1] to correct for neutron absorption and multiple scattering. The distributions have been arbitrarily extended to be symmetric with respect to 90°, since they are transitions between states of definite spin and parity. These figures are included principally to indicate the magnitude of the angular variation of the absorption corrections for our samples. Table I presents the co-

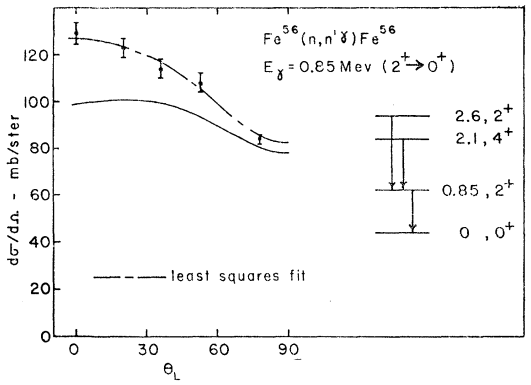

FIG. 7. Differential cross sections for the 0.85-Mev transition in Fe^{56}. The dot-dash curve is the least-squares fit to the measured cross sections. The solid curve represents the statistical model predictions. The low-energy portion of the Fe^{56} level scheme, with excited-state energy and spin and parity assignments, is shown at the right. Arrows indicate observed transitions.

efficients of a least-squares fit to the differential cross sections of the form

$$d\sigma/d\omega=a_0+a_2P_2+a_4P_4,$$

where the P_L are Legendre polynomials of order L. Curves are fitted after the data has been corrected for absorption.

Figures 7 through 12 present all of the differential cross sections measured as well as the results of our efforts to represent them with the statistical model. Low-energy portions of the nuclear level schemes are included in the figures to illustrate the levels participating in these transitions; arrows indicate measured transitions. The points are the measurements after absorption corrections have been applied, and the dot-dash curves are the least-squares fits whose coefficients

are tabulated in Table I. The solid and dashed curves are theoretical calculations of the differential cross sections using the neutron transmissions tabulated by Beyster *et al.*[7] The calculations include contributions through $l=3$ for both incident and outgoing neutrons for all transitions except those in Pb^{206}. The Pb^{206} calculations include terms through $l=4$.

The production cross sections for the 0.85-Mev line in Fe^{56} are presented in Fig. 7. This line is excited primarily by inelastic scattering to the 0.85-Mev state, but includes also cascade contributions from the 2.08- and 2.66-Mev states. Our measurements for this transition are in agreement with those of Hosoe and Suzuki,[3] where the measurements overlap. The solid curve was calculated from the assumed statistical model and includes calculated cascade contributions from the second and third excited states. The calculated second and third excited-state cascade contributions may be compared to measurements of them at 90°. The comparison is presented by comparing the experimental and theoretical ratios R_m and R_c of the cascade contributions to the

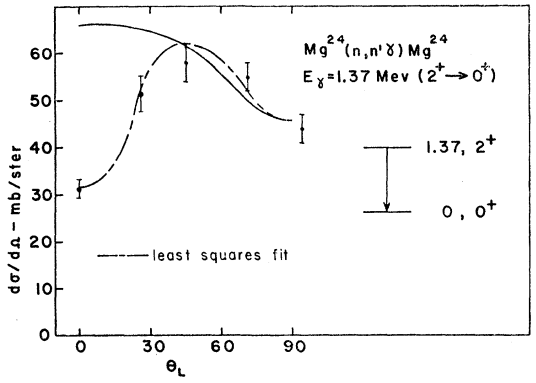

FIG. 8. Differential cross sections for the 1.37-Mev transition in Mg^{24}. The dot-dash curve is a least-squares fit to the measured cross sections. The solid curve represents the predictions of the statistical model. States of Mg^{24} participating in the transition are shown at the right.

total 90° production cross section for the 0.85-Mev line. For the cascade from the 2.08-Mev state, $R_c=6.1\%$ and $R_m=7.7\pm0.4\%$; for the cascade from the 2.66-Mev state, $R_c=11.8\%$ and $R_m=7.5\pm2.0\%$. These cascade contributions have also been measured by Van Patter and Jackiw,[5] with a gamma-ray detection system whose angular spread is ~40°. From their measurements, after corrections for angular spread have been applied, we find R_m values of 8.2% and 11.4% for the transitions from the 2.08- and 2.66-Mev states. The angular spread corrections are obtained from the statistical model predictions for the angular distributions.

The measurements and theoretical calculations for the indicated transition in Mg^{24} are shown in Fig. 8. These measurements are in good agreement with those of Hosoe and Suzuki for $\theta_L>45°$; their measurements do not include small angles. The model employed here

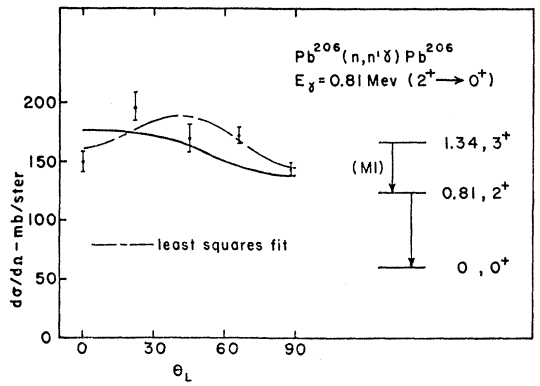

FIG. 9. Differential cross sections for the 0.81-Mev transition in Pb^{206}. The dot-dash curve is a least-squares fit to the measurements. The solid curve represents the statistical model calculations multiplied by 1.16. The low-energy portion of the Pb^{206} level scheme, with excited-state energy and spin and parity assignments, is shown at the right. Arrows indicate observed transitions. For the statistical model calculations of the 0.81-Mev transition, the $3^+ \rightarrow 2^+$ transition was assumed to be $M1$.

certainly does not properly represent the small-angle measurements, either for Fe^{56} or Mg^{24}. Since the Mg^{24} data showed such a pronounced anisotropy, we remeasured the angular region between 0° and 45° twice, and with two somewhat different experimental arrangements. The pulsed beam coincidence system measurements were repeated, and then the full beam was used with an associated particle coincidence system[14] to separate the gamma rays of interest. In the latter system, a thin anthracene detector was used to detect He^3 recoils from the $D(d,n)He^3$ source reaction and coincidences were required between the recoil He^3 particles and the prompt gamma rays. All measurements of the Mg anisotropy at small angles were in good agreement.

The measured and calculated cross sections for the Pb^{206} transitions are shown in Figs. 9 and 10. In contrast

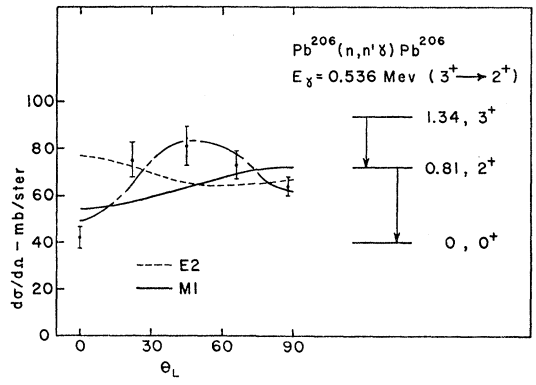

FIG. 10. Differential cross sections for the 0.536-Mev transition in Pb^{206}. The dot-dash curve is a least-squares fit to the measurements. The solid and dashed curves represent statistical model calculations for $M1$ and $E2$ multipolarities, respectively, multiplied by 1.56.

[14] R. C. Lamb, Technical Report UK-60-1 (Physics), 1960 (unpublished); Progress Report, under Atomic Energy Commission contract, 1961 (unpublished).

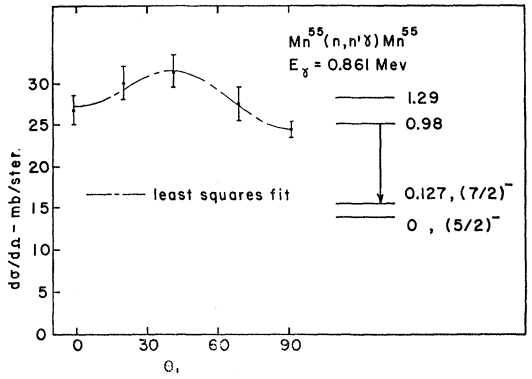

FIG. 11. Differential cross sections for the 0.861-Mev transition in Mn^{55}. The transition is indicated by an arrow in the level scheme shown at the right.

to the representations in Figs. 7 and 8, the solid curves of Figs. 9 and 10 are not the calculated differential cross sections, but differ from them by numerical factors. The solid curve of Fig. 9 represents the calculated cross sections multiplied by 1.16 and the curve in Fig. 10 is plotted to be the statistical model results multiplied by 1.56. As is apparent from the appearance of these factors, the agreement between calculated and measured cross sections for the 0.536-Mev transition is not especially satisfactory. Recently, the transition probabilities for excitation of the various states of Pb^{206} have been measured at 94° and as a function of neutron energy by Lind and Day.[15] Their report includes a decay scheme and branching ratios for the gamma-ray transitions; we have used this information to assist us in calculating the cross sections shown in Figs. 9 and 10. The solid curve of Fig. 9 includes the $3^+ \rightarrow 2^+$ cascade contribution from the 1.34-Mev state, assumed to be $M1$. The effect of the cascades from higher 2^+ states[15] on the shape of the curve has not been included, since the multipolarities of these cascade contributions are not known. These cascades account for 23% of the $2^+ \rightarrow 0^+$ transitions. However, the calculated differential cross sections have been adjusted in magnitude so that the total cross section does include the effects of the cascades from the higher 2^+ states. We have found that assuming $E2$ rather than $M1$ for the $3^+ \rightarrow 2^+$ transition does not appreciably alter the shape of the calculated distribution for the $2^+ \rightarrow 0^+$ line.

Figure 10 presents the measurements and calculations for direct excitation of the 3^+ state. There is no evidence[15] of cascades to this state from higher states, so that the calculations should completely represent this transition. The solid and dashed curves represent the assumptions $M1$ and $E2$, repsectively, for the $3^+ \rightarrow 2^+$ transition. Any admixture containing 20% or more $E2$ provides a distribution very similar to the dashed curve. The points plotted in Fig. 10 have been corrected for the expected 14% contribution to the measured yields from the 0.57-Mev line in Pb^{207}, assumed to be isotropic. A

[15] D. A. Lind and R. B. Day, Ann. of Phys. 12, 485 (1961).

TABLE II. Experimental and theoretical total cross sections for gamma-ray production.

Isotope	E_γ (Mev)	σ_m (mb)	σ_c (mb)
Fe^{56}	0.85 ±0.015	1260±60 1150±130[a] 1210[b]	1125
Mg^{24}	1.374±0.015	670±45 660±100[a]	697
Mn^{55}	0.861±0.007	356±20	
	1.18 ±0.010	310±20	
Pb^{206}	0.536±0.007	920±130[c] 500[d]	530
	0.814±0.010	2122±120 1500[d]	1670

[a] M. Hosoe and S. Suzuki, J. Phys. Soc. Japan 14, 699 (1959).
[b] D. M. Van Patter and R. W. Jackiw, *Proceedings of the International Conference on Structure, Kingston* (University of Toronto Press, Toronto, and North Holland Publishing Company, Amsterdam, 1960), p. 244.
[c] This value is obtained after subtracting the contribution of the Pb^{207} 0.57-Mev line from the measured yield. The quoted uncertainty does not include the uncertainty of this subtraction.
[d] D. A. Lind and R. B. Day, Ann. Phys. 12, 485 (1961).

general characteristic of the comparison of measured and calculated differential cross sections in Figs. 7 through 10 is that the measurements show more anisotropy than the model predicts.

Table II contains a summary of total cross sections obtained by integrating the measured differential cross sections and also those inferred from the statistical model. Energy measurements of the gamma rays are also included in this table. As shown in Table II, our measurements are in good agreement with the measurements of Hosoe and Suzuki[3] and Van Patter and Jackiw.[5] The present measurements of the Pb^{206} transition rates are not in agreement with those reported by Lind and Day.[15] A possible source of error could be our procedure for handling multiple scattering corrections. We adopted an approximate correction demonstrated by Day[1] to be valid for a somewhat different sample geometry than that used by us. Our Pb^{206} sample was a right circular cylinder of approximately 5.5-cm length and 1.9-cm diameter, oriented with cylinder axis perpendicular to the neutron flux. Day developed this approximation for the ring geometry. It would be difficult to attribute the

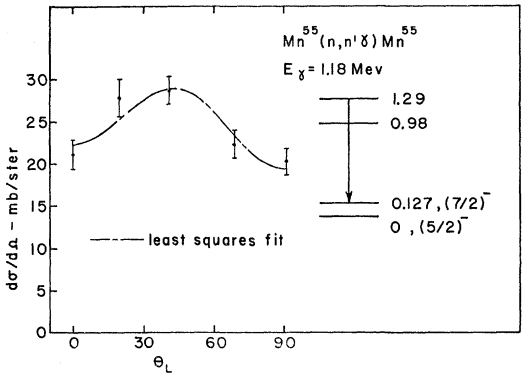

FIG. 12. Differential cross sections for the 1.18-Mev transition in Mn^{55}. The transition is indicated by an arrow in the level scheme shown at the right.

entire disagreement to this source, however, since the multiple scattering correction would be of the order of 17%. The theoretical cross sections in Table II are in agreement with the measured ones, except for our measurements for the 0.536-Mev line in Pb^{206}. Lind and Day had found that the cross sections implied by the neutron transmissions tabulated by Beyster *et al.*[7] were too large to represent the Pb^{206} transitions near threshold.[15] It is clear that this is not the case at this neutron energy; that is, the theoretical cross sections are not large compared to the measured ones.

Mn^{55} Levels

Differential cross sections of the $Mn^{55}(n,n'\gamma)$ lines from the second and third excited states have been measured in an effort to provide additional information about the properties of these states. Extensive measurements of $Mn^{55}(n,n'\gamma)$ cross sections have been reported and $Mn^{55}(n,n')$ differential cross sections have been measured at $E_n=2.45$ Mev.[4] Nath *et al.*[16] have compared their measurements as a function of neutron energy to theoretical expectations for Mn^{55} transitions in order to provide spin assignments of 9/2 and 11/2 to the second and third excited states, respectively. Their measurements did not fix the parities of these states. Figures 11 and 12 present differential cross sections for the production of gamma rays from the second and third excited states, respectively. The de-excitation of these levels is known[13,16] to proceed principally to the $\frac{7}{2}^-$ first excited state. The least-squares fits indicate significant P_4 coefficients for both distributions, which implies transition amplitudes of multipolarity $\geqslant 2$.

The degree of agreement between measured and computed total cross sections for $(n,n'\gamma)$ reactions indicated in Table II prompted us to use the statistical model described above to place limits on possible spin assignments to the levels of Mn^{55}. Unfortunately, the extent to which these states are indirectly excited by cascades from higher states is not known at $E_n=2.9$ Mev. It is not possible, therefore, to use the magnitudes of our production cross-section measurements to limit possible spins. Nath *et al.* have measured[16] the inelastic scattering cross sections to be 0.31 and 0.08 barn for the second and third excited states, respectively, at $E_n=2.47$ Mev. Cranberg and Levin[4] quote differential inelastic scattering cross sections of 20 and 11 mb/sr, respectively. If we assume isotropy for the inelastic neutron distributions, this would imply total cross sections of 0.25 and 0.14 barn. These measurements were at $E_n=2.45$ Mev. The size of the cross sections for excitation of the levels requires the spins to be $\leqslant 11/2$, and this together with the P_4 coefficients in our gamma-ray distributions indicates that a pronounced $E2$ amplitude is present in the second excited state transition, so that the parity of that state is odd, as expected by Nath *et al.* The statistical model employed in this paper yields cross sections of 180 and 113 mbarn for spins of $9/2^-$ and $11/2^-$. The principal argument in favor of a $9/2^-$ assignment for the second excited state was a single-particle branching ratio calculation[16] which assumed that the $9/2^-$ to $7/2^-$ transition was $M1$. Since we find a significant $E2$ amplitude is present in the transition, assignments of $\frac{7}{2}^-$ or $\frac{5}{2}^-$ might also be probable spins for that level. If we assume spins of $7/2^-$ and $11/2^-$ we calculate cross sections of 220 and 130 mbarns, respectively, in slightly better agreement with the observed cross sections and cross-section ratios. The statistical model predicts a rather small change in the cross-section magnitudes as the incident neutron energy is changed from 2.45 to 2.9 Mev. Our total production cross sections for the second and third levels are 356 and 310 mbarn, respectively, indicating considerable cascade contributions from higher states. For this reason, calculations of the differential production cross sections have not been attempted.

[16] N. Nath, M. A. Rothman, D. M. Van Patter, and C. E. Mandeville, Nuclear Phys. **13**, 74 (1961) and references cited therein.

ACKNOWLEDGMENT

The cooperation of R. C. Lamb, who remeasured the small-angle region of the $Mg^{24}(n,n'\gamma)$ distribution, is gratefully acknowledged.